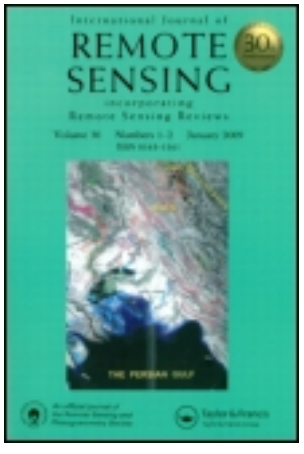

International Journal of Remote Sensing
Publication details, including instructions for authors and subscription information:
http://www.tandfonline.com/loi/tres20

Multi-type change detection of building models by integrating spatial and spectral information

Liang-Chien Chen [a], Chih-Yuan Huang [b] & Tee-Ann Teo [c]
[a] Centre for Space and Remote Sensing Research, National Central University, Jhong-Li, Taiwan
[b] Department of Geomatics Engineering, University of Calgary, Calgary, AB, Canada
[c] Department of Civil Engineering, National Chiao Tung University, HsinChu, Taiwan
Published online: 02 Nov 2011.

To cite this article: Liang-Chien Chen, Chih-Yuan Huang & Tee-Ann Teo (2012) Multi-type change detection of building models by integrating spatial and spectral information, International Journal of Remote Sensing, 33:6, 1655-1681, DOI: 10.1080/01431161.2011.593584

To link to this article: http://dx.doi.org/10.1080/01431161.2011.593584

International Journal of Remote Sensing
Vol. 33, No. 6, 20 March 2012, 1655–1681

Taylor & Francis
Taylor & Francis Group

Multi-type change detection of building models by integrating spatial and spectral information

LIANG-CHIEN CHEN*†, CHIH-YUAN HUANG‡ and TEE-ANN TEO§
†Centre for Space and Remote Sensing Research, National Central University, Jhong-Li, Taiwan
‡Department of Geomatics Engineering, University of Calgary, Calgary, AB, Canada
§Department of Civil Engineering, National Chiao Tung University, HsinChu, Taiwan

(*Received 19 August 2010; in final form 3 April 2011*)

Detecting building changes followed by updates is preferable for efficient revisions to building models. Additionally, more change types can be detected with spatial information provided by building models for reducing land surveying work. Therefore, for efficient building of model revision and land surveys, this work applies a new multi-type change detection scheme with new light detection and ranging (LIDAR) point clouds, new aerial images and existing building models. By integrating the spatial information from LIDAR data and image-based spectral information, this work identifies changes to existing buildings and identifies newly built and changed buildings. To provide an initial value for further revisions, new building regions are generated from change detection results. Experimental results demonstrate that the proposed scheme has high accuracy for both change type determination and building region generation. To provide comprehensive observations, experimental results deemed unreliable are scrutinized.

1. Background

Three-dimensional (3D) building models have numerous applications, such as in layout planning for cellular radio networking (Siebe and Buning 1997), urban planning, construction and management (Danahy 1999). Photo-textured 3D building models are used for visual 3D browsing (Volz and Klinec 1999). The most common visualization applications are Google Earth and Microsoft Bing Map. In the field of photogrammetry, 3D building models can be used for true orthorectification of aerial imagery (Rau 2002).

In response to the increasing requirements of building modelling, many investigations have been published. Zhang and Gruen (2006) reconstructed building models using stereo-image matching. Multi-source data are commonly combined for model reconstruction; for example, light detection and ranging (LIDAR) and aerial imagery (Huber *et al*. 2003), LIDAR and vector maps (Taillendier 2005) and aerial imagery and vector maps are often combined (Suveg and Vosselman 2004). However, due to the variety and complexity of buildings, the accuracy in automatically reconstructing building models may not be adequate for technical applications (Taillendier

*Corresponding author. Email: lcchen@csrsr.ncu.edu.tw

International Journal of Remote Sensing
ISSN 0143-1161 print/ISSN 1366-5901 online © 2012 Taylor & Francis
http://www.tandf.co.uk/journals
http://dx.doi.org/10.1080/01431161.2011.593584

2005). Thus, high-cost and low-efficiency semi-automatic reconstruction procedures are commonly applied to increase precision of building model.

However, building models must inevitably be updated. Since unchanged buildings do not require updating, it is preferable to first identify changed buildings and then update these buildings. Therefore, detecting changes in building models is a task important to efficient revision.

In addition to revision purposes, change detection can be utilized for land surveys, development assessments and property monitoring. These applications are especially suited to crowded areas, which typically have many illegal buildings or extensions, resulting in destruction of the urban landscape, safety concerns and tax-evasion problems. However, in the literature, due to insufficient input data (e.g. two-dimensional (2D) maps), change classes/types are often classified as 'changed' (which is sometimes further separated into 'new' and 'demolished') or 'unchanged'. The change detection result then requires many human analyses to generate applicable data. Conversely, building models provide more spatial information for change detection than 2D maps. Using height difference is easier than analysing 2D shape difference in generating many detailed change types, such as extensions, reconstruction or demolition. This can markedly decrease the amount of human work needed by existing techniques.

Additionally, since the first step in constructing a building model is usually to find an area of building, if building regions can be directly generated based on the change detection result, this will benefit the subsequent revision process. Tracing building boundaries from LIDAR data involves vector-based and raster-based approaches. In vector-based approaches, Sampath and Shan (2007) traced boundaries with the angles between LIDAR points; Xu *et al.* (2010) extracted boundaries by analysing height differences among vertices and relationships between triangulated irregular network (TIN) facets; and Wang and Schenk (2000) extracted boundaries by intersecting the planar segments in TIN. In raster-based approaches, Masaharu and Hasegawa (2000) and Rottensteiner and Briese (2002) generated boundaries by plane segmentation on a digital surface model (DSM). Four point-to-region methods (two are developed in this work) are analysed and compared in this work. Among the four methods, three are vector-based and one is raster-based. The comparison of these methods will be useful for any study generating regions from LIDAR point clouds.

In generating a building region, we assume that land cover consists primarily of buildings, vegetation and ground (including water) (Rottensteiner *et al*. 2007). To identify buildings, vegetation and ground areas must be detected. In the literature, vegetation and ground areas may cause change detection errors because they have a similar height or spectrum signature to buildings (Knudsen and Olsen 2003, Vu *et al*. 2004). Therefore, for change detection and building region generation, both vegetation and ground must be detected.

For land surveys and building model revisions, this work applies a new scheme to identify in detail change classes/types and generates new building regions. Data from two epochs are used in this work. The new epoch data contain LIDAR point clouds and multi-spectral imagery when building models are in the previous epoch.

2. Literature review

This literature review first analyses existing change detection approaches according to their strategies, data sets and unit types. The most suitable scheme for the objectives in this work is then adopted.

2.1 *Strategies*

Two change detection strategies are available. The first one performs classification and then compares class similarities between two epochs. Several studies have adopted this strategy (Knudsen and Olsen 2003, Matikainen *et al*. 2004, Walter 2004, Champion *et al*. 2008). The advantage of this strategy is that training data can be extracted from the existing data. Additionally, if the same units (e.g. the same polygons) are used in classification, changes can be identified by simply comparing classes in two epochs. However, this strategy is highly dependent upon classification results and identifying changes in the same class that have different attributes is difficult (e.g. a building after the construction of micro-structures, such as a staircase, is still a building).

The second strategy detects changes via attribute differences (e.g. height and grey levels) between two epochs. This strategy has fewer omission errors than the former strategy because it does not have the mentioned issues caused by classification (Murakami *et al*. 1999, Jung 2004, Zhu *et al*. 2009). However, this strategy can only determine similarities between two epochs, not the semantic meaning of a change. For instance, when comparing building height in two epochs, a building (assume known) with reduced height in the new epoch may be a demolished building or a reconstructed building. Notably, this strategy can only determine that building heights differ. However, this limitation can be overcome by using additional rules based on prior knowledge. For instance, if the height of a building in the new epoch is the same as ground height, the building is a demolished building.

Most data in the literature, such as geographic information system (GIS) layers or vector maps, contain insufficient information for identifying attribute differences. Therefore, previous investigations often used the first strategy, such as Knudsen and Olsen (2003), Matikainen *et al.* (2004) and Walter (2004). However, 3D building models provide accurate height information, which facilitates calculation of height differences. Thus, the second strategy is preferable for reducing omission errors. Notably, some rules must be set based on prior knowledge to obtain semantic classes.

2.2 *Data sets*

The information required for change detection can be divided into spectral and spatial information. Spectral information is the intensity of spectral values of image bands, which are usually from multi-spectral imagery. As mentioned, vegetation areas typically cause change detection errors (Knudsen and Olsen 2003). Vegetation indices, which are calculated based on radiance values in certain bands, can be applied to detect vegetation areas and reduce the number of errors. In this situation, true orthorectification is desirable for integrating detected vegetation areas and 3D building models. However, misclassification can occur when a ground area has spectral reflection similar to that of a building (Knudsen and Olsen 2003, Vu *et al*. 2004). One solution to this problem is to apply normalized DSMs (nDSMs); the ground areas can be detected easily by setting a height threshold on nDSMs.

Spatial information conveys 2D (such as edges in an image) and 3D information. The 3D spatial information describes relief in the real world, such as that in DSMs, nDSMs, digital elevation models (DEMs) and digital building models (DBMs). The LIDAR system can efficiently generate a large amount of spatial data. As mentioned, spatial information can be applied to detect ground areas efficiently. However, in addition to problems associated with LIDAR point density, imprecise building boundaries

and interpolation error, the primary problem is that vegetation areas are hard to detect using LIDAR data/DSMs (Vu *et al*. 2004, Champion *et al*. 2008). Conversely, vegetation can be detected easily using spectral information.

Although vegetation and ground areas cause change detection errors (Knudsen and Olsen 2003), these errors can be avoided by detecting vegetation and ground areas using spectral and spatial information, respectively. Therefore, multi-spectral imagery and LIDAR point clouds are applied to reduce the magnitude of change detection errors in this study.

2.3 *Unit types*

The units used in change detection are mainly points (such as pixels) and areas (such as polygons). Using points as the principal unit facilitates detection of detailed changes; however, it is hard to link with other points for more reliable detection. Many schemes use points as the change detection unit in, say, pixel-based comparisons between classes in two periods (Knudsen and Olsen 2003), comparisons between point clouds (Girardeau-Montaut *et al*. 2005) and subtraction between DSMs from two epochs (Murakami *et al*. 1999, Vu *et al*. 2004).

When using area as the unit, one can discreetly determine changes by including information associated with other units. For instance, Walter (2004) identified changes by studying average of grey values, roof slope and the coverage ratio of vegetation and ground within a polygon. Since using area as the unit directs to more reliable change detection (Li *et al*. 2010), many investigators have tried to generate area unit from imagery or LIDAR data (Matikainen *et al*. 2003, 2004, Vögtle and Steinle 2004, Vu *et al*. 2004, Bouziani *et al*. 2007, Im *et al*. 2008). However, the problem in using area as the primary unit is that minor classes in a polygon may be overlooked.

Since building models consist of polygons, area can be used as the unit for discrete change detection. To deal with the problem of overlooked minor classes, rule-based change classes/types determination is adopted. For instance, a micro-structure-changed building can be found by setting a rule, that is, if the changed percentage in the building is smaller than 50% and the changed area in the building is larger than 25 m^2, the building is 'micro-structure changed'.

3. Objectives

For land surveys and building model revisions, this work integrates new LIDAR point clouds, new multi-spectral aerial images and existing 3D building models for building change detection. A change detection method for determining multiple change types is needed. In generating new building regions, different point-to-region methods are analysed and compared.

4. Methodologies

This work has five major stages: (1) data preprocessing; (2) change type determination for original buildings; (3) detection of newly built and changed buildings; (4) generation of building regions in the new epoch; and (5) validation of proposed scheme. The data sets used in this work include existing epoch building models (without texture), new epoch LIDAR point clouds and new epoch aerial images with exterior orientation parameters. The images contain red (R), green (G) and blue (B) data and near infrared (NIR) bands corrected by true orthorectification. The building models consist

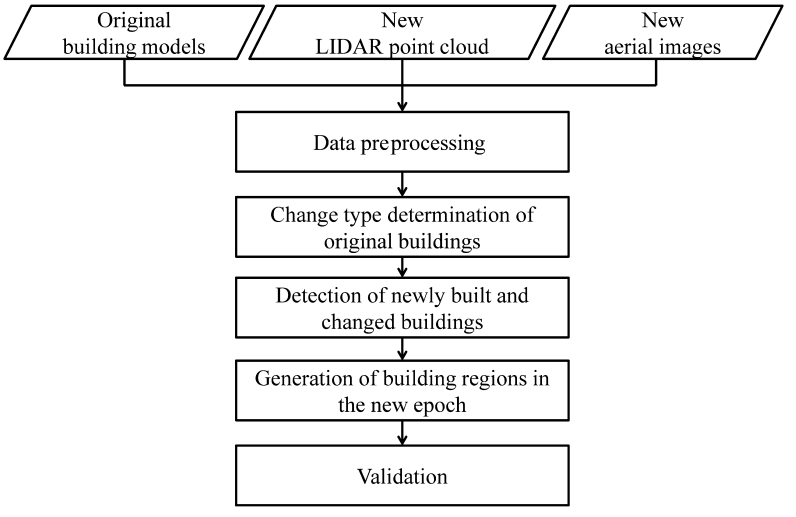

Figure 1. Workflow of the proposed scheme.

of vector elements, which consist of ordered 3D vertexes. The LIDAR data are 3D discrete point clouds. Figure 1 shows the proposed workflow.

4.1 *Data preprocessing*

During data preprocessing, the information required for change detection and building region generation is produced. As mentioned, ground and vegetation areas are needed for change detection and building region generation. Additionally, to identify multiple change types, the change ratio and area of each building model polygon are required. Hence, this work calculates height differences between new LIDAR points and existing 3D building models and obtains the distribution of changed points for deriving change ratio and area. The principal purpose of this step is to generate a ground index map, vegetation index map and changed points.

Before generating the required information, the DSMs, DEMs and nDSMs are produced from LIDAR point clouds by TerraScan (Terrasolid 2010). All data sets are then co-registered via manually measured control points. To generate a ground index map, we assume that the height of every structure exceeds 2 m. Thus, pixel values in the nDSMs lower than 2 m are ground.

During vegetation index map generation, normalized difference vegetation index (NDVI) is applied to detect vegetation at non-occluded areas in aerial images. However, for occluded areas in images, texture information of relief is used to detect vegetation because no spectral information can be utilized. First, this work generates grey-level co-occurrence matrix textures (Curran 1988) of the nDSMs. These textures are then used as input in maximum likelihood-based supervised classification with vegetation areas detected by NDVI as training data. Therefore, the vegetation index map is generated by combining the areas detected by NDVI and areas detected by classification.

To prevent errors arising from ground and vegetation areas, these areas are removed from LIDAR data before generating change points. However, some non-roof points may remain, which are primarily LIDAR points on a wall. These wall points must be

removed because they can result in incorrect height differences. Detection and removal of wall points are accomplished by Delaunay triangulation and removing the lowest point in vertical triangles. The reason that the highest point is not removed is that a sufficient number of points remain.

The height difference between two epochs can then be calculated with the remaining LIDAR points and building models. With the building model surface equation, a vertical/height distance between LIDAR point and building model surface can be derived. With this height difference, changed points are identified using the following rule. If the distance between a LIDAR point and building model exceeds the height of a floor (set at 3 m here), it is a changed point. The distribution of changed points and unchanged points is then generated.

4.2 *Change type determination of original buildings*

A building model is a digital model representing a building in the real world, which can be composed of multiple 3D polygons. These polygons can represent a building's roof or wall. This work only applies polygons representing roof surfaces, which are called elements in this article. A building model element consists of ordered 3D vertexes, which can be used in calculating height difference between two epochs or percentage of different classes in the element. As mentioned, using area as a unit in change determination is reliable by including more information. This work determines change types based on building model elements (a building may have several elements), meaning that each element has its own change type.

As mentioned, building changes were simply classified as 'changed' or 'unchanged'; however, relatively greater detail is needed. With the increasing LIDAR point density and the spatial information of 3D building models, micro-structure changes can be identified, as with the proposed scheme. Therefore, this work first discusses change types that should be addressed in building changes (e.g. micro-structure changes).

Building changes can be simply divided into changes to an original building and newly constructed buildings. Changes to original building structures are classified as the following three types: (1) buildings that have been replaced, which are defined as 'main-structure changed'; (2) construction or demolition of a micro-structure, which is defined as 'micro-structure changed'; and (3) buildings that have been torn down, which are defined as 'demolished'. Additionally, changes in buildings that are occluded, such as by a tree, are clearly difficult to detect by remote sensing. Therefore, this work defines buildings occluded by vegetation as 'vegetation-occluded' buildings. The 'demolished' and 'vegetation-occluded' buildings can be identified by ground and vegetation areas, respectively. The 'main-structure-changed' buildings can be identified by the change ratio of each building model polygon, which can be derived from height difference between two epochs. To distinguish 'micro-structure-changed' buildings from 'main-structure-changed' buildings, this work applies the amount of change area of each building model polygon, which can also be derived from height difference between two epochs.

Additionally, new building is defined as 'newly built'. Overall, building change types in this work are as follows: 'unchanged'; 'main-structure changed'; 'micro-structure changed'; 'demolished'; 'vegetation occluded'; and 'newly built'. Figure 2 shows the relationships of these change types.

To determine change type, one must identify the difference between change types. Besides, using area as a unit provides the ability to include more information. This

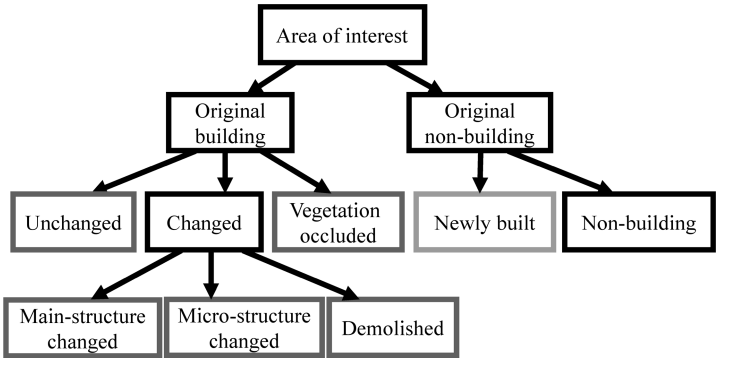

Figure 2. Relationships of change types.

work compares the following four attributes: height in the new epoch; NDVI in the new epoch; percentage of changed points in a building model element; and changed area in a building model element. The percentage of changed points in a building model element is the number of changed points in an element divided by the total number of LIDAR points in the same element. The changed area equals the percentage of changed points multiplied by the total area of the element.

Table 1 compares change types. In table 1, '–' indicates that the attribute has uncertain characteristics. For instance, following building demolition, the NDVI can be high for growing vegetation or low for bare soil. Such uncertainty and similarity between 'unchanged' and 'micro-structure changed' can generate errors during statistical classification. Thus, instead of using a statistics-based approach, this work uses a rule-based process. With a rule-based approach, the drawback of using area as a unit (minor class may be overlooked, which is 'micro-structure changed' in this work) can also be addressed.

The rules for identifying change types are as follows. The detection of a demolished building can be done by assessing its height in the new epoch (table 1). Notably, a vegetation-occluded building can be identified by NDVI. The building attributes of 'unchanged' and 'main-structure changed' are more obvious than 'micro-structure changed', and can be determined by the percentage of changed points. Since 'micro-structure-changed' buildings only have partial changes, they are hard to distinguish from 'main-structure-changed' and 'unchanged' buildings by the percentage of changed points. However, since 'micro-structure-changed' buildings have a noticeable amount of changed area, they can be determined by change areas after

Table 1. Comparison of change types.

	Unchanged	Main-SC	Micro-SC	VO	Demolished
Height in new epoch	High	High	High	High	Low
NDVI in new epoch	Low	Low	Low	High	–
Ratio of changed points	Low	High	Low	–	High
Changed area	Low	High	Middle	–	High

Notes: '–' indicates that the attribute has uncertain characteristics; NDVI, normalized difference vegetation index; SC, structure changed; VO, vegetation occluded.

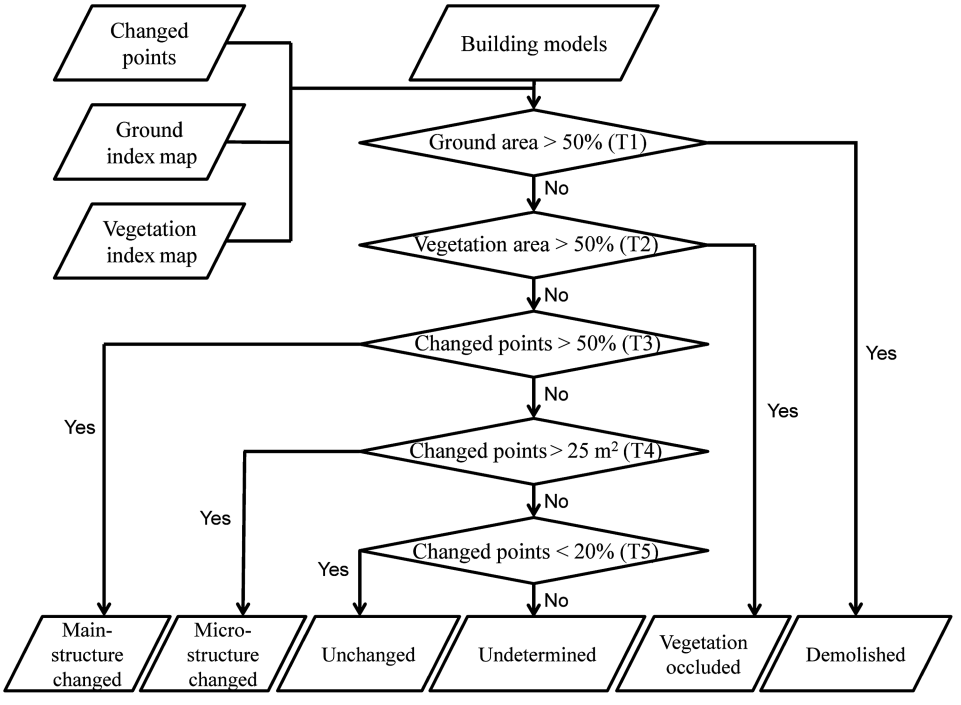

Figure 3. Workflow of change type determination on original buildings.

filtering 'main-structure-changed' buildings, which can be identified by the percentage of changed points. Therefore, these rule-based determinations should have a certain sequential workflow. The rules for determining the change types can be seen in figure 3. 'Demolished', 'vegetation occluded', 'main-structure changed', 'micro-structure changed' and 'unchanged' are mainly related to percentage of ground, percentage of vegetation, percentage of changed points, changed area and percentage of changed points in a building model element, respectively, where T1–T5 are set thresholds.

The following statements lead to the sequence of these determinations. Since a 'demolished' building has uncertain NDVI attributes, its identification should be before that of 'vegetation-occluded' buildings, or 'demolished' buildings may be misclassified. For the same reason, 'vegetation-occluded' buildings should be detected before 'unchanged', 'main-structure-changed' and 'micro-structure-changed' buildings because of the uncertainty in the changed points percentage and changed area. 'Main-structure-changed' buildings should be identified prior to that of 'micro-structure-changed' buildings, or 'main-structure-changed' buildings may be classified as 'micro-structure changed' when change area exceeds the change area threshold (T4 in figure 3). Moreover, the percentage of changed points for 'micro-structure-changed' buildings can be low for large building elements. Thus, the 'micro-structure-changed' determination should be processed before the 'unchanged' determination.

Therefore, this work develops a new rule-based sequential determination scheme for identifying change types. The determination sequence is as follows: (1) 'demolished'; (2) 'vegetation occluded'; (3) 'main-structure changed'; (4) 'micro-structure changed'; and (5) 'unchanged'. If an element cannot be categorized, it is considered

an undetermined element. Additionally, if an element is too small (<2 m^2) or has few points (<4 points), it is a 'lack-of-data' situation.

The process of setting thresholds for each rule is described as follows. First, if ground area covers more than half of the area of an element (T1), the element is classified as 'demolished'. Second, if vegetation area covers more than half of the area of an element (T2), the element is classified as 'vegetation occluded'. When half of the points belong to changed points in an element (T3), the element is classified as a 'main-structure-changed' element. This work considers micro-structures larger than 5 m × 5 m, meaning the threshold is 25 m^2 for identifying 'micro-structure-changed' elements (T4). Finally, because commission errors can be manually post-processed but omission errors cannot be restored, a relatively more discrete threshold is needed for identifying 'unchanged' buildings. Therefore, when the percentage of changed points is <20% (T5), an 'unchanged' building is identified. Figure 3 shows the workflow and thresholds. Notably, these thresholds are based on prior knowledge, which can be altered with different perspective.

4.3 *Detection of newly built and changed buildings*

In this work, we assume land cover types are mainly buildings, vegetation and ground (Rottensteiner *et al*. 2007). Once vegetation and ground areas are removed from the second epoch LIDAR points, the remaining points should belong to buildings in the second epoch. These remaining points consist of unchanged buildings, newly built buildings, changed buildings and noises. Via the change type determination of first epoch buildings, unchanged building elements are detected. The points which fall into unchanged buildings can be removed. Moreover, the noise points are some discrete points or thin lines due to registration error. To remove this noise, first the region growing/grouping process is applied. Beginning with any un-grouped point, if points locate in a growing range, these points are set as the same group as the beginning point. Then other un-grouped points that locate in the growing range of those previously grouped points are grouped. If no more points can be grouped, re-process the procedure with any un-grouped point as the beginning point. After all, all points can be grouped. Since noises are often in small groups, noises can be removed by elimination of groups with few points. Therefore, after removing vegetation areas, ground areas, unchanged building areas and noises from the second epoch LIDAR points, the remaining points can be considered newly built or changed building points.

4.4 *Generation of building regions in the new epoch*

Since the first step in constructing a building model is typically identifying building regions, if regions can be generated using the change detection result, building detection can be ignored in the subsequent revision process. In the data sets generated in previous steps, 'unchanged' building elements and newly built or changed building points are regarded as new epoch buildings. Since 'unchanged' elements and newly built or changed points are of different types (elements and points), finding regions based on different types is difficult. Therefore, points that are inside and near 'unchanged' elements' edges are created for representing these elements. Then these points are combined with newly built or changed points. Furthermore, to avoid influences from other buildings, the region growing process is applied to group building points.

Four approaches are analysed to generate regions from discrete points. Three vector-based approaches are used to trace the boundary of discrete points, and one raster-based approach is applied to generate regions directly from discrete points. The three boundary tracing methods are the angle method (Sampath and Shan 2007), the TIN method (Teo *et al*. 2007) and the TIN-constrained angle method. The first method, the angle method, determines boundary points based on the angle between discrete points; the TIN method extracts the boundary from the connection among points in a TIN; and the third method, the TIN-constrained angle method, detects a boundary based on the angle between connected points. The raster-based method finds the building region by searching for building pixels in both row and column directions following rasterization; this method is called the maximum & minimum method. The TIN-constrained angle method and maximum & minimum method are novel methods.

4.4.1 Angle method (Sampath and Shan 2007)**.** Figure 4 shows an application of the angle method. One starts from the left-most point and searches for the next point within a set range (grey circle in the first column of figure 4). Because more than one point exists in this circle, an angle for each possible point (angle shown in the second and third columns of figure 4) is calculated. The point with the smallest angle is then deemed a boundary point (the fourth and fifth columns of figure 4). However, the actual process is relatively more complex. If no candidate points exist in the search range, the search range expands. If the search range has been enlarged to a certain length threshold and no candidate point has been discovered, delete the last traced boundary point and return to the previous boundary point for finding another candidate.

4.4.2 TIN method. The TIN method is based on the work by Teo *et al.* (2007). First Delaunay triangles are constructed, and the three links in each triangle are recorded. The boundary links are recorded only once and inner links are recorded twice. Thus, the inner links can be detected and removed easily. However, detecting and removing inner links of TIN yields a traced boundary that is always a convex hull, which cannot

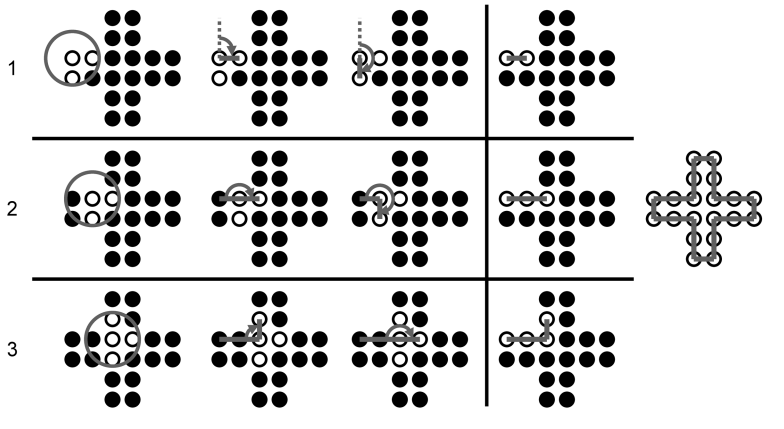

Figure 4. Angle method procedure (Sampath and Shan 2007).

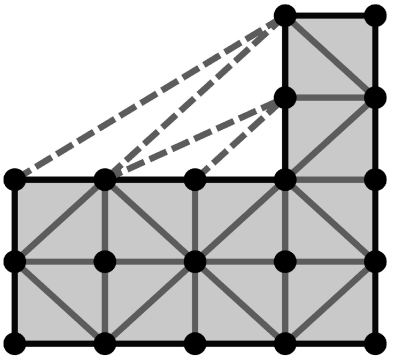

Figure 5. An example of the triangulated irregular network (TIN) method (grey area, building; dash links, non-boundary links; light grey solid links, inner links; black solid links, building boundary).

be applied to non-convex hull buildings. Through observations, a building (grey area in figure 5) that is far from a convex hull has non-boundary links and most are long (dash links in figure 5). Therefore, the TIN method first removes the triangles with long links by setting a length threshold. Inner links (light-grey solid links in figure 5) are then removed by detecting links shown twice. Therefore, the building boundary can be generated (black links in figure 5). However, because some non-boundary links are short (e.g. the shortest dash link in figure 5), these links may remain after long links are removed. This will generate an extracted boundary that is slightly larger than the actual building region.

4.4.3 TIN-constrained angle method. In the TIN-constrained angle method, a boundary is determined by the angle method and the selection of candidate points based on the TIN connection relationship. The procedure starts from the left-most point, as does the angle method. The point with a TIN connection relationship is selected (as in the TIN method, the link must exceed the length threshold) and then the next boundary point with the smallest angle is found. If no candidate points exceed the length threshold, the threshold will be enlarged or the traced boundary will revert to the previous boundary point, as does the angle method. Since no need exists to search for candidate points, the TIN-constrained angle method is faster and has a lower likelihood of tracing an incorrect boundary than the angle method.

4.4.4 Maximum & minimum method. The maximum & minimum method is inspired by the scan line grouping approach (Hatger and Brenner 2003). First, rasterization is employed for transforming points into grid (figure 6(*a*)). Then, the method searches 'column-wisely' for the first and last columns containing building pixels in each row (dark-grey pixels in figure 6(*b*)) and fills in pixels between the two columns (light-grey pixels in figure 6(*b*)). The dark-grey and light-grey areas are then regarded as building areas derived by the column-wisely search (figure 6(*b*)). Similarly, this method conducts a row-wisely search for the first and last rows that contain building pixels in each column (dark-grey pixels in figure 6(*c*)) and fills in pixels between the two rows (light-grey pixels in figure 6(*c*)). The dark-grey and light-grey areas are

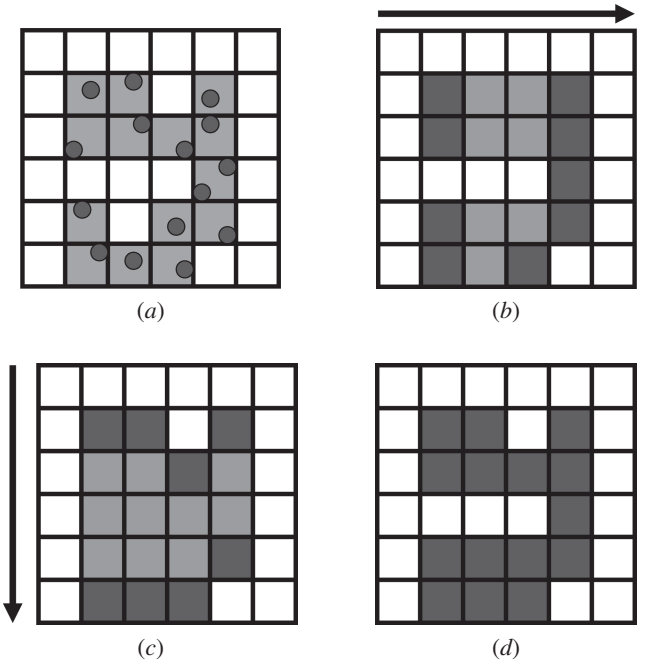

Figure 6. An example of the maximum and minimum method. (*a*) Rasterization. (*b*) Column-wisely search. (*c*) Row-wisely search. (*d*) Intersection (final) result.

then considered building areas derived from row-wisely search result (figure 6(*c*)). The final building region is extracted by taking the intersection of the column-wisely search result and the row-wisely search result (figure 6(*d*)).

Additionally, since boundary details are usually parallel or perpendicular to the major axis of a building, relatively better results can be obtained after resampling rasterized building pixels to the major building axis. This method is faster than other methods and a building region can always be found when building pixels exist. However, errors are related to pixel size used in rasterization, and the double-indented structure cannot be completely extracted (compare the fifth row and third column in figure 6(*a*) and (*d*)).

4.5 *Validation*

The results of change type determination for original buildings and generation of new epoch building regions are validated. To validate the change type determination, building elements are randomly selected and the change types are manually determined by comparing aerial images for two epochs. Overall accuracy, omission error, commission error and the Kappa index are calculated (Congalton 1991). Calculations of the combined and individual Kappa indices in this work are based on the method developed by Cohen (1960).

To validate the building region generation result, reference data are needed. This work manually measures changed building regions from stereo-images, and then combines measured regions with unchanged building regions as reference data. Experimental results are examined based on both pixel and region for a thorough

understanding. First, extracted boundary and reference data are rasterized into 0.5 m × 0.5 m pixels. Then, in pixel-based validation, the experimental result and reference data are compared on a pixel-by-pixel basis. The overall accuracy, omission error, commission error and Kappa index are then calculated. In region-based validation, when half of the area of a reference building element is covered by extracted building regions, the reference building element is detected; otherwise, this is an omission error. A commission error occurs when an extracted building region does not cover a reference building element. Since the non-building area cannot be validated by region-based validation, only omission and commission errors are calculated.

5. Experimental results

5.1 *Test data*

The original 3D building models were obtained in 2002, while the LIDAR point clouds and aerial images were acquired in 2005. The building models were obtained from 1:5000 stereo-aerial images and contain the 3D coordinates of roof corner points. Figure 7 shows the building models. The LIDAR point clouds were acquired using a Leica ALS50 (Leica Geosystems AG, Heerbrugg, St. Gallen, Switzerland) with a density of 1.7 points/m^2. The elevation range in this data set is 87–191 m. The planimetric and height accuracies are 0.60 and 0.15 m, respectively (Leica-Geosystems 2006). Figure 8 shows the DSM produced from LIDAR point clouds. Eight aerial images are utilized in this work; these aerial images were acquired by an UltraCamD (Vexcel Imaging GmbH, A-8010 Graz, Austria) with a focal length of 101.4 mm at a flight height of 1300 m. The spatial resolution is 12 cm for the R, G, B and NIR bands. The root mean square error (RMSE) of exterior orientation parameters in the planimetric position and height are 0.3 and 0.7 m, respectively.

The test site, which is in HsinChu City, northern Taiwan, has factories, business buildings and residential areas. Thus, the test site is suitable for evaluating the proposed scheme for a variety of building types. Figure 9 depicts the mosaicked aerial images and outlines the test area with bold lines. This test site is 1 km × 2 km in area.

Figure 7. The 3D building models in HsinChu City, Taiwan.

Figure 8. Digital surface model (DSM) (light detection and ranging (LIDAR) data).

Figure 9. Mosaicked aerial images and outlined test area.

The reference data for validation of change type determination contain 378 'unchanged', 12 'main-structure-changed', 10 'micro-structure-changed', 15 'demolished' and 19 'vegetation-occluded' building elements.

5.2 *Validation of change type determination*

Figure 10 shows change type determination results. Blue, red, maroon, purple, green, grey and cyan represent the 'unchanged', 'main-structure-changed', 'micro-structure-changed', 'demolished', 'vegetation-occluded', 'undetermined' and

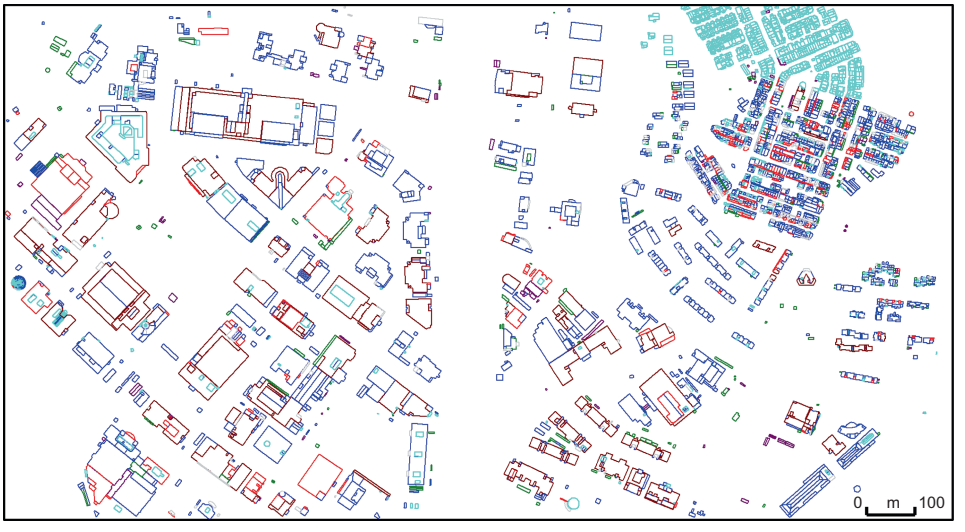

Figure 10. Change type determination results (blue, unchanged; red, main-structure changed; maroon, micro-structure changed; purple, demolished; green, vegetation occluded; grey, undetermined; cyan, lack of data).

Table 2. Error matrix.

	Reference						
Results	UD	Unchanged	Main-SC	Micro-SC	Demolished	VO	Total
UD	0	23	0	0	0	0	23
Unchanged	0	288	1	0	0	0	289
Main-SC	0	10	9	0	0	0	19
Micro-SC	0	19	0	9	0	0	28
Demolished	0	0	0	0	15	0	15
VO	0	5	0	0	0	19	24
Total	0	345	10	9	15	19	398
Total number of correctly determined elements							340

Note: UD, undetermined; SC, structure changed; VO, vegetation occluded.

Table 3. Accuracy indices.

	Unchanged	Main-SC	Micro-SC	Demolished	VO	Total
Overall accuracy (%)	–	–	–	–	–	85.4
Omission error (%)	16.5	10.0	0.0	0.0	0.0	5.3
Commission error (%)	0.4	52.6	67.9	0.0	20.8	28.3
Kappa coefficient	0.40	0.90	1.00	1.00	1.00	0.60

Note: SC, structure changed; VO, vegetation occluded.

'lack-of-data' elements, respectively. Table 2 shows the error matrix excluding 'lack of data' (Congalton 1991). Table 3 lists the accuracy indices. Analytical results have an overall accuracy up to 85%. But the commission error rate is 28%; one reason is because the number of changed buildings in this data set is much smaller than

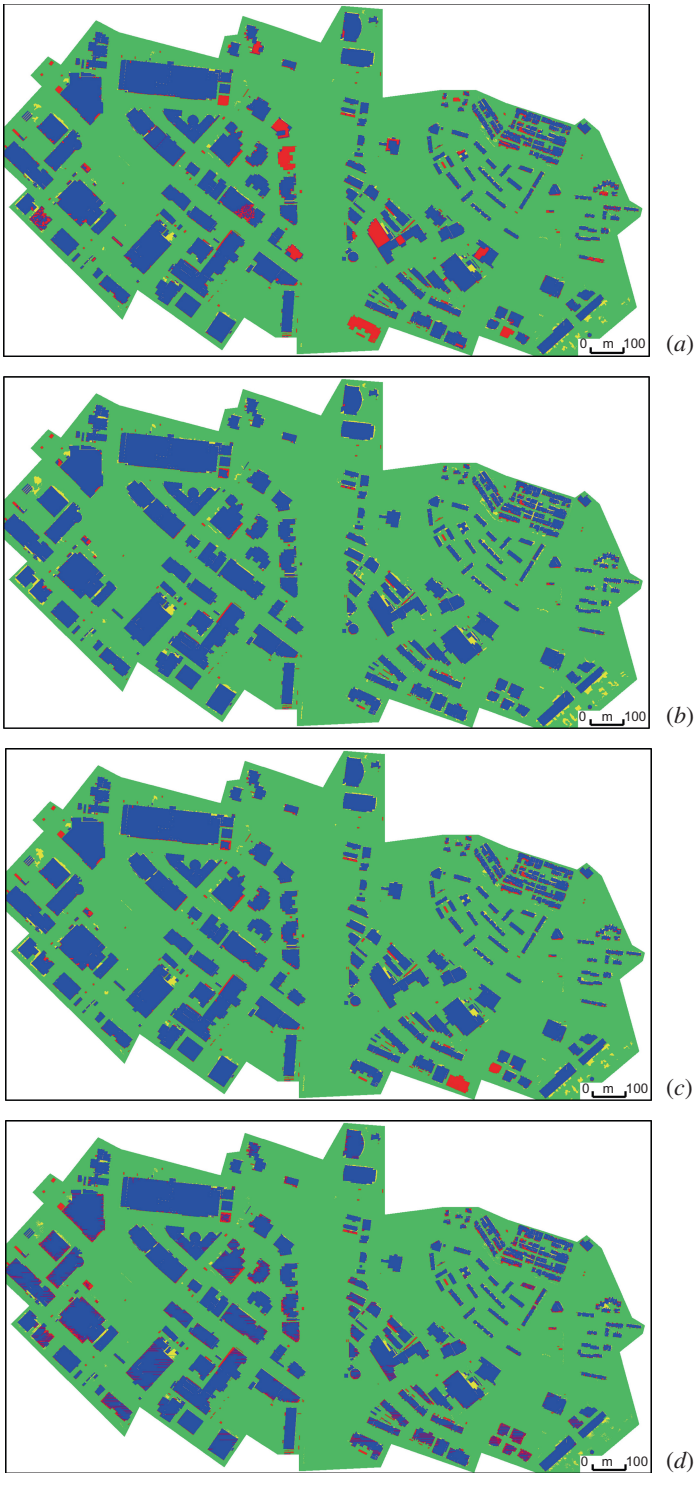

Figure 11. Pixel-based validation of building region generation. (*a*) Angle method. (*b*) Triangulated irregular network (TIN) method. (*c*) TIN-constrained angle method. (*d*) Maximum & minimum method (blue, both reference and result are buildings; green, both reference and result are non-buildings; red, omission error; yellow, commission error).

the number of unchanged buildings. Another reason is that the real roof surfaces of building models cannot be accurately delineated. For instance, water towers or air-conditioner cooling towers are not included in the building models. All possible error factors found are discussed in §6.4.

5.3 *Validation of building region generation*

Figure 11 shows pixel-based validation results. The blue area indicates that both experimental results and reference data are building pixels, green means both are non-building pixels, red indicates that it is a building pixel in reference data but a non-building pixel in experimental result (omission error) and yellow means a non-building pixel in reference data but a building pixel in experimental result (commission error). Table 4 lists the calculated accuracy indices of pixel-based validation.

Figure 12 shows region-based validation results. The blue area indicates a correctly discovered building, red indicates an omission error and green indicates a commission error. Table 5 shows the commission and omission errors of region-based validation.

This work then compares the experimental results of the four building region generation methods. Although both the angle method and TIN-constrained angle method can generate more precise boundaries than the other two, some buildings are missed because these two methods directly trace on the irregular LIDAR points. Conversely, since the TIN and maximum & minimum methods generate regions from Delaunay triangles and raster data, the boundary is not as precise as that with the angle method and the TIN-constrained angle method. As mentioned, the TIN method slightly enlarges extracted regions. Additionally, because of the influence of gaps between discrete LIDAR points and the set grid size when processing rasterization, some regions generated by the maximum & minimum method are broken into pieces (i.e. the lower right section in figure 11(*d*)).

This work now discusses calculated accuracy indices. Since non-building areas are larger than building areas in the test site, calculated indices may be optimistic in pixel-based validation. Conversely, because of randomly distributed LIDAR points, some edge areas of buildings are hard to detect. Then these undetectable areas could easily become a majority in small elements (i.e. the residential area in the upper-right section of test data set). Therefore, omission error may be too pessimistic in region-based validation. Although both pixel-based and region-based validations have weaknesses, the TIN method can find most building regions, as indicated by experimental results and accuracy indices. Additionally, even if the TIN method has the most commission errors because the extracted region is slightly enlarged, this work is primarily concerned with omission errors. The error factors causing omission and commission errors are discussed in §5.4.

Table 4. Accuracy indices for building region generation (pixel-based).

	Overall accuracy (%)	Commission error (%)	Omission error (%)	Kappa coefficient
Angle method	95.3	6.0	12.8	0.90
TIN method	96.5	8.7	4.6	0.91
TIN-constrained angle method	96.5	6.5	7.2	0.91
Maximum & minimum method	95.7	6.4	10.8	0.89

Note: TIN, triangulated irregular network.

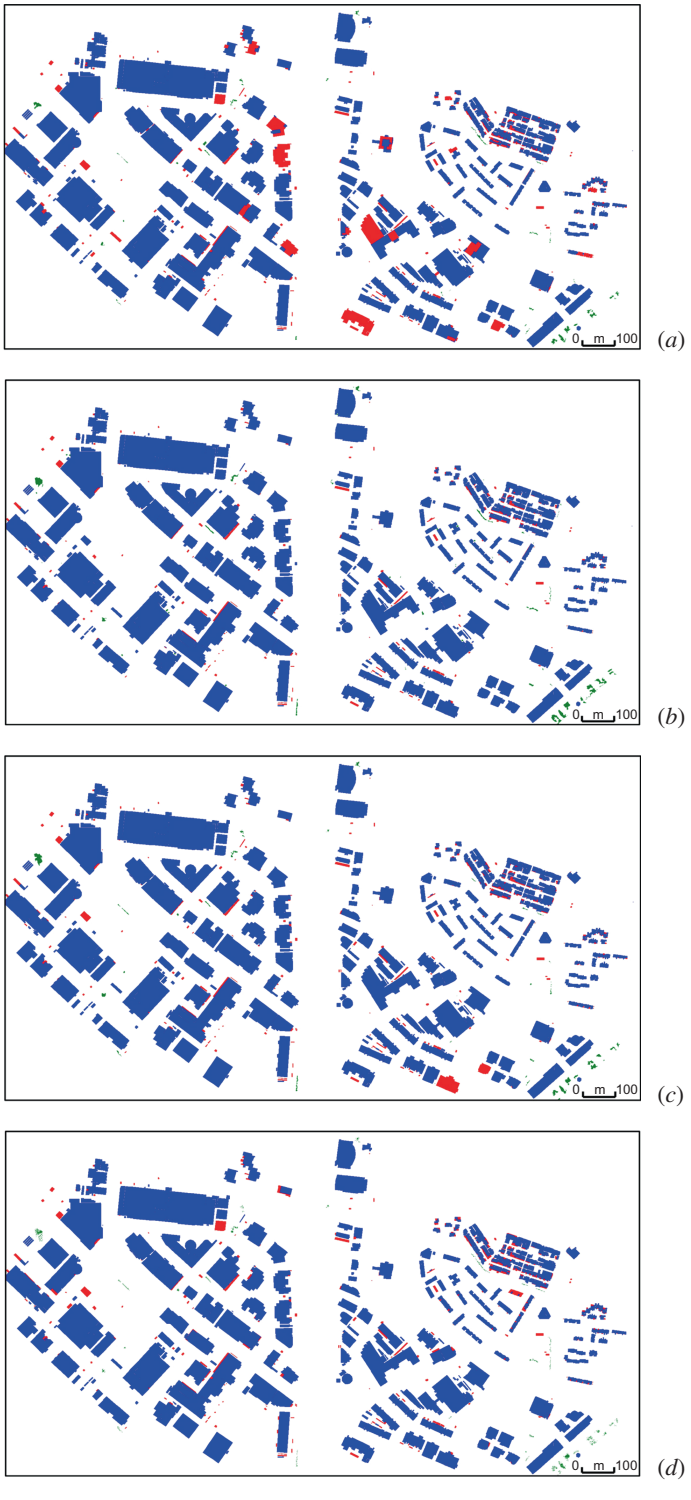

Figure 12. Region-based validation of building region generation. (*a*) Angle method. (*b*) Triangulated irregular network (TIN) method. (*c*) TIN-constrained angle method. (*d*) Maximum & minimum method (blue, correctly discovered buildings; red, omission error; green, commission error).

Table 5. Accuracy indices for building region generation (region-based).

	Commission error (%)	Omission error (%)
Angle method	2.5	21.3
TIN method	4.0	12.9
TIN-constrained angle method	2.1	16.8
Maximum & minimum method	2.0	19.5

Note: TIN, triangulated irregular network.

5.4 *Analysis of error factors*

The factors causing errors in change type determination and building region generation are described in this section. Among the four generated building region results, the TIN method result is selected for analysis.

5.4.1 Error factor analysis for change type determination. In change type determination, seven error factors are found. Table 6 lists the error factors, number of cases and descriptions (figures 13 and 14).

Table 6. Error factors in change type determination.

Type	Number of cases	Description
1. High wall points	18	Since this work did not remove the high wall points because the LIDAR points in some building model element may be insufficient, these high wall points adversely affect the determination result
2. Imprecise building models	15	Building models cannot accurately delineate the real world. For instance, parapets or micro-structures, such as water towers, air conditioners and staircases, are often omitted in original building models. Figure 13 shows a parapet, and figure 14 shows pipes and air conditioners. The red and green points in figures 13(*b*) and 14(*b*) indicate changed points and unchanged points, respectively
3. Small elements	12	Small elements have few LIDAR points for determining change type; thus, they will be categorized in the 'lack-of-data' category
4. Partly vegetation-occluded elements	5	The removal of LIDAR points in vegetation areas can result in an insufficient number of points for determining change
5. Lack of LIDAR points	1	Because some materials do not reflect LIDAR signals, elements constructed of these materials are classified in the 'lack-of-data' category
6. Courtyards	1	Elements representing courtyards are classified in the 'lack-of-data' category because LIDAR points in the vegetation and ground areas are removed
7. Changed element with a small height difference	1	Since height difference is one of the principal information in change type determination, errors may occur when changed elements have small height differences

Note: LIDAR, light detection and ranging.

(*a*) (*b*)

Figure 13. An example of 'imprecise of building models'-parapet. (*a*) Aerial image. (*b*) Changed points (blue, building boundary; red, changed points; green, unchanged points).

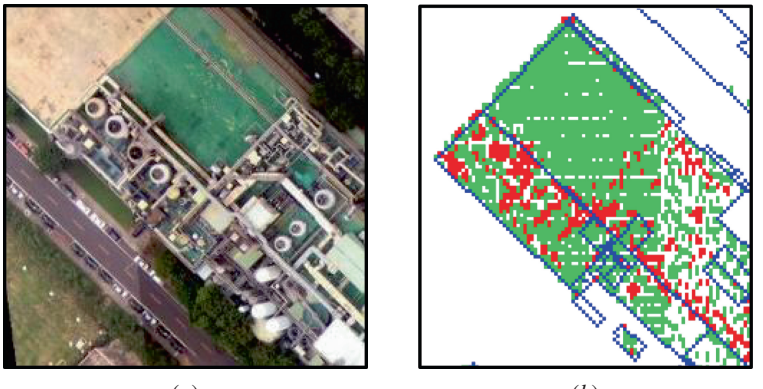

(*a*) (*b*)

Figure 14. An example of 'imprecise of building models' pipes and air conditioners. (*a*) New aerial image. (*b*) Changed points (blue, building boundary; red, changed points; green, unchanged points).

5.4.2 Error factor analysis of building region generation. This work analyses the error factors causing omission errors and commission errors in building region generation. Table 7 shows the error factors causing omission errors (figure 15), and table 8 shows the error factors causing commission errors (figure 16).

5.5 *Classification of error factors*

To discover the possible solutions of error factors, this work categorizes error factors into three classes – 'method limitation', 'data limitation' and 'data quality issue'. If error factors can be solved by modifying or extending the proposed method, they belong to 'method limitation'. Error factors influenced by data characteristics belong to 'data limitation'. Errors that can be reduced by improving data quality are categorized as a 'data quality issue'. Table 9 shows the classification of error factors. Table 10 depicts the number of each error factor cases.

In total, 38%, 32% and 30% of errors fall into the 'method limitation', 'data limitation' and 'data quality issue' categories, respectively. The 'method limitation' and

Table 7. Error factors in building region generation: omission errors.

Type	Number of cases	Description
8. Vegetation-occluded elements	30	Since points in vegetation areas are removed, buildings occluded by vegetation cannot be found. Figure 15(*a*) depicts an example
9. Building with few LIDAR points	14	Small elements, elements partly occluded by vegetation or low LIDAR point densities result in insufficient information for generating building regions. Figure 15(*b*) depicts an example
10. Ground detection errors	6	The LIDAR points can pass through some roof materials and record the heights of inner structures, which can cause errors during ground detection. Figure 15(*c*) depicts an example
11. Lack of LIDAR points	6	The occlusion effect or absorption of energy by roof materials can result in the loss of LIDAR points. In this case, new building regions cannot be generated. Figure 15(*d*) depicts an example
12. Vegetation detection error in occluded areas	3	Since no spectral information can be utilized for vegetation detection in occluded areas of aerial images, this work uses textures of nDSM in classification to compensate for these areas. However, the classification result is not as good as that using NDVI. Therefore, some incorrectly detected vegetation areas result in the removal of additional LIDAR points

Note: LIDAR, light detection and ranging; NDVI, normalized difference vegetation index; nDSM, normalized digital surface model.

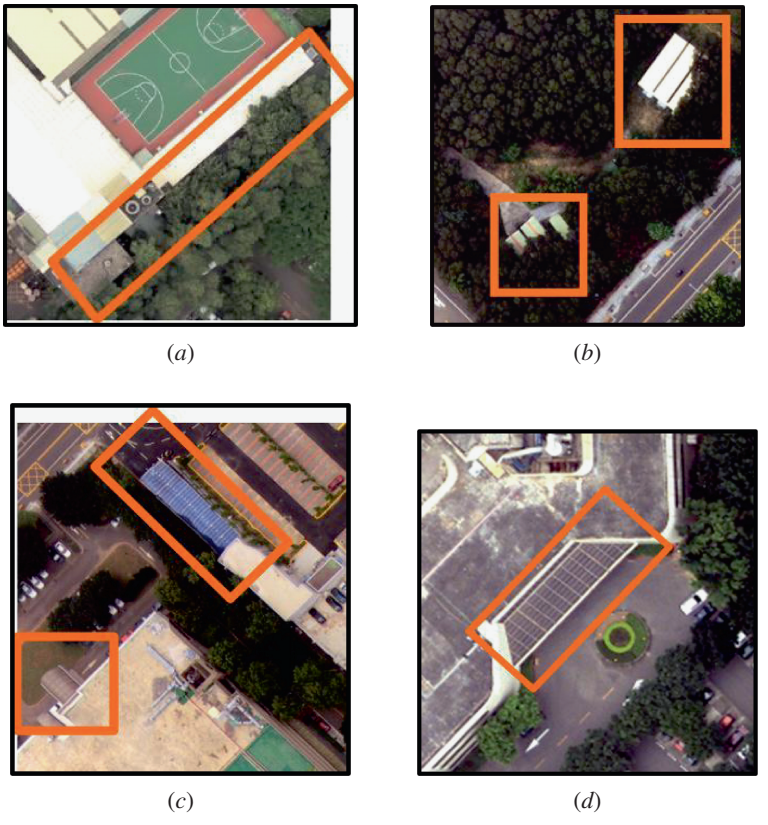

Figure 15. Omission error examples in building region generation. (*a*) Vegetation occluded. (*b*) Few light detection and ranging (LIDAR) points. (*c*) Ground detection error. (*d*) Lack of LIDAR points.

'data quality issue' errors are much easier to resolve than 'data limitation' errors. If both the method and data quality are improved, the number of errors can be reduced by at most 68%.

6. Conclusions

For building model revision and land survey, this work proposed a new scheme that detects changes in old building models with new LIDAR point clouds and aerial imagery. With the proposed method, multiple change types can be generated to reduce human determination work while surveying land. Additionally, the new epoch building regions generated provide good initial values for building model revisions.

The overall accuracy of change type determination was as high as 85%. The influence of ground and vegetation during change detection can be decreased by integrating spatial and spectral information. To generate building regions, the TIN method performs best out of the four methods with this test data, with an overall accuracy as high as 96% in pixel-based validation. However, vegetation-occluded and non-building objects are primary sources of errors during region generation.

Table 8. Error factors in building region generation: commission errors.

Type	Number of cases	Description
13. Non-building objects	27	Some man-made non-building structures are misrecognized as buildings, such as containers, trucks, high-voltage towers and carports
14. Ground detection errors	9	This error typically occurs in areas with parking ramps or revetments
15. Close buildings	3	If buildings are closely packed, the generated region may combine buildings
16. Non-building points around buildings	2	If non-building points near a building are missed during the removal process, the generated building region may be enlarged slightly
17. Occlusion detection errors	2	Since this work uses DSM in image true orthorectification and DSM cannot delineate building boundaries well, the true orthorectification result may have some errors around building boundaries. Normally, when this error occurs at a ground area, the LIDAR points can still be removed using the ground index map. However, when this error occurs in areas with vegetation, LIDAR points remain and are misrecognized as buildings. Figure 16 depicts an example
18. Vegetation detection errors	1	Some vegetation cannot be detected by NDVI and cause vegetation detection error. These vegetation areas will be misrecognized as buildings

Note: LIDAR, light detection and ranging; NDVI, normalized difference vegetation index; DSM, digital surface model.

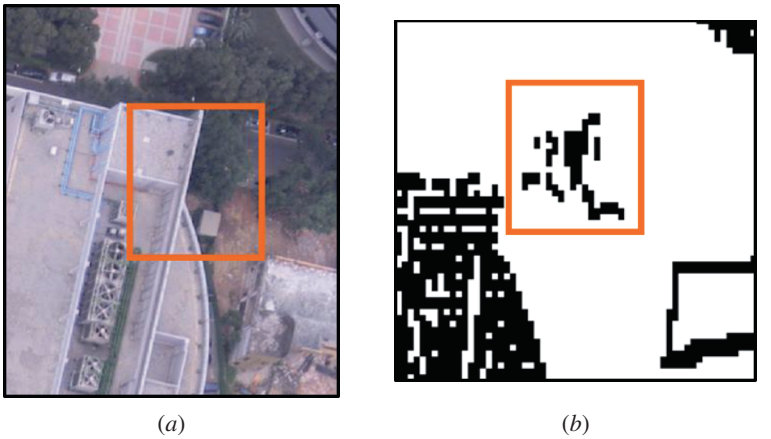

(*a*) (*b*)

Figure 16. An example of 'occlusion detection errors'. (*a*) Aerial image. (*b*) Input data for region generation.

Through careful observation and classification of error factors, this work elucidates the problems that may be encountered during change detection of building models and region generation from discrete points. Besides the aforementioned solutions for method limitation, a possible improvement for proposed change detection scheme is reducing the sensitivity of rule-based threshold by integrating with probability theory

Table 9. Classification of error factors.

Error factor*	Class	Reasons
1.	ML	The high wall points can be deleted during the wall point removal process
2.	DQI	These errors can be resolved when building models can delineate real roofs in an acceptable accuracy. Conversely, the proposed scheme may be used for assessing building model completeness
3.	DQI	This error is due to the LIDAR point density problem. With increased point density, this error factor can be resolved
4.	DL	If a building is occluded by another object, no data can be used for detecting changes. This occlusion typically occurs in remote sensing and photogrammetry fields
5.	DL	This error occurs for occluded areas in a LIDAR point cloud or un-reflecting infrared roofs
6.	ML	The proposed scheme does not consider building elements representing courtyards. Although this error is not easily resolved, courtyards are rare
7.	ML	This error occurs because the proposed scheme uses height difference between two epochs as one of the principal information for change detection. This error may be resolved by applying edge detection on images to match with building model edge. In addition, if the original building model contains texture information, image correlation between two epochs can be applied
8.	DL	The reason for this error is the same as that for error type 4—partly vegetation-occluded elements error
9.	DQI	The reason for this error is the same as that for error type 3—small elements
10.	DL	The reason for this error is that the LIDAR points pass through some roof materials
11.	DL	The reason for this error is the same as that for error type 5—lack of LIDAR points
12.	DQI	Since the outcome of using nDSM textures for detecting vegetation is poor, if occluded areas in images when taking aerial photos can be reduced in size, the incidence of this error can be reduced
13.	ML	This error can be resolved by differentiating building and non-building objects with additional rules or information
14.	ML	This error is caused by ramps. Although this error is closely related to the ground definition, this error may be solved by modifying the DEM generation method
15.	ML and DQI	Although difficult, this error may be solved by choosing a relatively better grouping threshold or method before generating building regions. Furthermore, higher LIDAR point density also allow better grouping
16.	ML	Although this error is usually caused by vegetation detection error or occlusion detection error, it may be solved by regularizing the generated building boundary
17.	DL	Since DSMs cannot delineate building boundaries well, using DSMs in true orthorectification has poor accuracy
18.	DL	This error occurs because some vegetation cannot be found by vegetation indices

Notes: ML, method limitation; DQI, data quality issue; DL, data limitation; nDSM, normalized digital surface model; DEM, digital elevation model; LIDAR, light detection and ranging; DSM, digital surface model.
*The error factors referred to are listed in tables 6–8.

Table 10. Number of error factor cases.

Class	Error factors	Number	Total
Limitation of method	1. High wall points	181127932	61
	6. Courtyard		
	7. Changed element with a small height difference		
	13. Non-building objects		
	14. Ground detection errors		
	15. Close buildings		
	16. Non-building points around buildings		
Limitation of data	4. Partly vegetation-occluded elements	51306621	51
	5. Lack of LIDAR points		
	8. Vegetation-occluded elements		
	10. Ground detection errors		
	11. Lack of LIDAR points		
	17. Occlusion detection errors		
	18. Vegetation detection errors		
Data quality issue	2. Imprecise building models	15121433	47
	3. Small elements		
	9. Building with few LIDAR points		
	12. Vegetation detection error in occluded areas		
	15. Close buildings		

Note: LIDAR, light detection and ranging.

(e.g. fuzzy set theory). Therefore, for elements that cannot clearly fit into any change type, further determination with including more information (e.g. line features from imagery) could be helpful.

Acknowledgement

The authors thank National Science Council and Ministry of the Interior of Taiwan for their support.

References

Bouziani, M., Goita, K. and He, D.C., 2007, Change detection of buildings in urban environment from high spatial resolution satellite images using existing cartographic data and prior knowledge. In *International Geoscience and Remote Sensing Symposium*, 23–28 July 2007, Barcelona (Piscataway, NJ: IEEE International) pp. 2581–2584.

Champion, N., Matikainen, L., Rottensteiner, F., Liang, X. and Hyyppa, J., 2008, A test of 2D building change detection methods: comparison, evaluation and perspectives. *International Archives of the Photogrammetry, Remote Sensing and Spatial Information Sciences*, **37**, pp. 297–304.

Cohen, J., 1960, A coefficient of agreement for nominal scales. *Educational and Psychological Measurement*, **20**, pp. 37–46.

Congalton, R.G., 1991, A review of assessing the accuracy of classifications of remotely sensed data. *Remote Sensing of Environment*, **37**, pp. 35–46.

Curran, P.J., 1988, The semivariogram in remote sensing: an introduction. *Remote Sensing of Environment*, **24**, pp. 493–507.

Danahy, J, 1999, Visualization data needs in urban environmental planning and design. In *Proceedings of Photogrammetric Week*, 22–26 September 1999, Stuttgart (Heidelberg: Wichmann Verlag), pp. 351–365.

Girardeau-Montaut, D., Roux, M., Marc, R. and Thibault, G., 2005, Change detection on points cloud data acquired with a ground laser scanner. *International Archives of the Photogrammetry, Remote Sensing and Spatial Information Sciences*, **36**, pp. 30–35.

Hatger, C. and Brenner, C., 2003, Extraction of road geometry parameters from laser scanning and existing databases. In *ISPRS Working Group III/3 Workshop '3-D Reconstruction from Airborne Laserscanner and InSAR Data'*, 8–10 October 2003, Dresden, Germany (Dresden: Institute of Photogrammetry and Remote Sensing, Dresden University of Technology), pp. 225–230.

Huber, M., Schickler, W., Hinz, S. and Baumgartner, A., 2003, Fusion of LIDAR data and aerial imagery for automatic reconstruction of building surfaces. In *Proceedings of 2nd GRSS/ISPRS Joint Workshop on Data Fusion and Remote Sensing over Urban Areas*, 22–23 May 2003, Berlin (Piscataway, NJ: IEEE press), pp. 82–86.

Im, J., Jensen, J.R. and Tullis, J.A., 2008, Object-based change detection using correlation image analysis and image segmentation. *International Journal of Remote Sensing*, **29**, pp. 399–423.

Jung, F., 2004, Detecting building changes from multitemporal aerial stereopairs. *ISPRS Journal of Photogrammetry and Remote Sensing*, **58**, pp. 187–201.

Knudsen, T. and Olsen, B.P., 2003, Automated change detection for updates of digital map databases. *Photogrammetric Engineering and Remote Sensing*, **69**, pp. 1289–1296.

Leica-Geosystems, 2006, Leica Geosystems brochure of ALS50-II. Available online at: http://gi.leica-geosystems.com/default.aspx (accessed 10 May 2010).

Li, P., Xu, H. and Guo, J., 2010, Urban building damage detection from very high resolution imagery using OCSVM and spatial features. *International Journal of Remote Sensing*, **31**, pp. 3393–3409.

Masaharu, H. and Hasegawa, H., 2000, Three-dimensional city modeling from laser scanner data by extracting building polygons using region segmentation method. *International Archives of Photogrammetry and Remote Sensing*, **33**, pp. 556–562.

Matikainen, L., Hyyppä, J. and Hyyppä, H., 2003, Automatic detection of buildings from laser scanner data for map updating. *International Archives of the Photogrammetry, Remote Sensing and Spatial Information Sciences*, **34**, pp. 218–224.

Matikainen, L., Hyyppä, J. and Hyyppä, H., 2004, Automatic detection of changes from laser scanner and aerial image data for updating building maps. *International Archives of the Photogrammetry, Remote Sensing and Spatial Information Sciences*, **35**, pp. 434–439.

Murakami, H., Nakagawa, K., Hasegawa, H., Shibata, T. and Iwanami, E., 1999, Change detection of buildings using an airborne laser scanner. *ISPRS Journal of Photogrammetry and Remote Sensing*, **54**, pp. 148–152.

Rau, J.Y., 2002, Geometrical building modeling and its application to the ortho-rectification for aerial images. PhD thesis, National Central University, Taiwan.

Rottensteiner, F. and Briese, C., 2002, A new method for building extraction in urban areas from high-resolution LIDAR data. *International Archives of Photogrammetry and Remote Sensing*, **34**, pp. 295–301.

Rottensteiner, F., Trinder, J., Clode, S. and Kubik, K., 2007, Building detection by fusion of airborne laser scanner data and multi-spectral images: performance evaluation and sensitivity analysis. *ISPRS Journal of Photogrammetry and Remote Sensing*, **62**, pp. 135–149.

Sampath, A. and Shan, J., 2007, Building boundary tracing and regularization from airborne LIDAR point clouds. *Photogrammetric Engineering and Remote Sensing*, **73**, pp. 805–812.

Siebe, E. and Buning, U., 1997, Application of digital photogrammetric products for cellular radio network planning. In *Proceedings of Photogrammetric Week*, 22–26 September 1997, Karlsruhe, Germany (Heidelberg: Wichmann Verlag), pp. 159–164.

Suveg, I. and Vosselman, G., 2004, Reconstruction of 3D building models from aerial images and maps. *ISPRS Journal of Photogrammetry and Remote Sensing*, **58**, pp. 202–224.

TAILLENDIER, F., 2005, Automatic building reconstruction from cadastral maps and aerial images. *International Archives of Photogrammetry and Remote Sensing*, **36**, pp. 105–110.

TEO, T.A., CHEN, L.C., RAU, J.Y. and CHEN, S.J., 2007, Building reconstruction using a split-shape-merge method. *Asian Journal of Geoinformatics*, **7**, pp. 31–34.

TERRASOLID, 2010, TerraScan user's guide. Available online at: http://www.terrasolid.fi/system/files/tscan_1.pdf (accessed 25 October 2010).

VÖGTLE, T. and STEINLE, E., 2004, Detection and recognition of changes in building geometry derived from multitemporal laser scanning data. *International Archives of Photogrammetry and Remote Sensing*, **35**, pp. 428–433.

VOLZ, S. and KLINEC, D., 1999, Nexus: the development of a platform for location aware application. In *Proceedings of 3rd Turkish-German Joint Geodetic Days*, Vol. 2, 1–4 June 1999, Istanbul (Istanbul: Istanbul Technical University), pp. 599–608.

VU, T.T., MATSUOKA, M. and YAMAZAKI, F., 2004, LIDAR-based change detection of buildings in dense urban areas. *IEEE International Geoscience and Remote Sensing Symposium*, **5**, pp. 3413–3416.

WALTER, V., 2004, Object-based classification of remote sensing data for change detection. *ISPRS Journal of Photogrammetry and Remote Sensing*, **58**, pp. 225–238.

WANG, Z. and SCHENK, T., 2000, Building extraction and reconstruction from lidar data. *International Archives of Photogrammetry and Remote Sensing*, **33**, Amsterdam, The Netherlands, unpaginated CD-ROM.

XU, J.Z., WAN, Y.C. and YAO, F., 2010, A method of 3D building boundary extraction from airborne LIDAR points cloud. *Photonics and Optoelectronics*, pp. 1–4.

ZHANG, L. and GRUEN, A., 2006, Multi-image matching for DSM generation from IKONOS imagery. *ISPRS Journal of Photogrammetry and Remote Sensing*, **60**, pp. 195–211.

ZHU, L., SHIMAMURA, H., TACHIBANA, K., LIU, Z. and GONG, P., 2009, Building change detection using aerial images and existing 3D data. *Urban Remote Sensing Event*, pp. 1–5.